ON THE EVALUATION OF DRYOUT CONDITIONS FOR A HEAT-RELEASING POROUS BED IN A WATER POOL[1]

S. E. Yakush[1,2], P. Kudinov[3]

[1]Ishlinskiy Institute for Problems in Mechanics RAS
Ave. Vernadskogo 101 Bldg 1, Moscow, 119526, Russia
[2]Moscow Institute of Physics and Technology
9 Institutsky per., Dolgoprudny, Moscow Region, 141701, Russia
yakush@ipmnet.ru

[3]Division of Nuclear Engineering, Royal Institute of Technology (KTH)
Roslagstullsbacken 21, C3, Stockholm, 106 91, Sweden
pkudinov@kth.se

ABSTRACT

This work is motivated by the problem of restraining temperature escalation inside a porous heat-releasing media submerged in a pool of liquid coolant. When coolant temperature reaches saturation, boiling begins in the bulk of the porous bed, with void generation rate determined by the heating power. Amount of void determines hydrostatic pressure difference that drives natural circulation of two-phase flow through the porous material. At a certain critical value of the heat release rate, the driving head cannot overcome drag of the two phase porous media flow, which results in complete evaporation of coolant in some zone. Temperature of material in the dry zone increases significantly due to deterioration of heat exchange with single phase vapor flow in comparison with boiling flow heat transfer. The paper considers the problem of determining the critical conditions for onset of dryout in a heat-releasing porous bed of an arbitrary shape. The well-known one-dimensional problem for a flat top-flooded bed is revisited, and the functional form of the dryout boundary (expressed as the dryout heat flux, DHF) is derived using non-dimensional parameters. Asymptotic behavior of the solution is analyzed, and, by the method of asymptotic interpolation, a surrogate model is proposed consisting of three single-argument, non-dimensional functions. It is shown that such a model provides acceptable accuracy even in the cases where complete similarity of solutions is not achieved. The results obtained provide important insights into the physics of the problem, reduce the number of free parameters, and enable fast evaluation of dryout conditions without the need of numerical solution of algebraic equations involved in the exact formulation. The ultimate goal of the surrogate model development, i.e. its application to multidimensional configurations, is discussed.

KEYWORDS

Two-phase flow; porous bed; coolability; dryout; severe accident

Corresponding author: S.E.Yakush, e-mail: yakush@ipmnet.ru

1. INTRODUCTION

Studies of water cooling of an internally heated porous bed are to a large extent motivated by nuclear power plant safety problems. In the event of a severe accident caused by failure of reactor fuel cooling function, core degradation and relocation of molten core materials (corium) into the lower plenum of reactor pressure vessel can occur, which can then result in subsequent vessel failure, as was the case in the severe accident at Fukushima Dai-Ichi power plant on March 11th 2011 [1].

In many reactor designs, most notably in Nordic-type boiling water reactors (BWRs) [2], a deep water pool in the reactor cavity is available as a design feature intended to prevent direct thermal attack on the containment floor and penetrations (doors, cable openings etc.) by the molten corium released from the vessel. Provided that the pool is deep enough, melt-water interaction results in corium fragmentation, quenching and formation of a porous debris bed on the pool floor (containment basemat).

Short-term cooling of high-temperature melt is achieved by the removal of the latent heat stored in the corium material and bringing the particle surface temperature close to the saturation temperature of coolant corresponding to the local hydrostatic pressure. However, there also exists a continuous source of material heating due to radioactive decay (so-called decay heat) persisting at quite high levels (~megawatts) for a long time (days, months). If decay heat cannot be removed, gradual material reheating will bring its temperature to high values at which exothermal chemical reactions can start, or even remelting of corium can occur. High temperature (~2000-3000K) molten debris attack on the containment structures poses immediate threat to the containment integrity. The coolability problem, thus, is to provide conditions under which the decay heat released in the corium is transferred to the pool of water in natural circulation conditions for a long enough period to maintain the material temperature at low levels and, therefore, to arrest the accident progression.

Water evaporation is the principal heat transfer mechanism by which the decay heat released in corium particles can be removed from the bulk of porous bed. This mechanism is efficient as long as all the porous material remains wetted by water supplied by filtration through the outer boundary of the bed. The coolant flow rate is determined by the balance between void generated in the bed (and thus hydrostatic pressure difference) and two phase flow drag in porous media. If the heat release rate exceeds some critical value, driving head becomes insufficient and a dry zone filled with steam can appear. In this zone, the temperature of solid material starts to grow due to the imbalance between decay heat release and heat removal. The temperature of debris can be stabilized eventually, but at much higher values determined by the efficiency of single phase heat transfer from debris to steam.

Research into the conditions under which dryout can occur, depending on porous bed properties (particle diameter, porosity), system pressure and bed geometry was first focused on a one-dimensional configuration with water fed into the bed either on top, or with additional bottom feeding [3, 4, 5, 6, 7, 8, 9, 10]. The models derived were considering the balance between the vapor and liquid flows in the bed, the main differences being in the formulation of two-phase drag laws (including the porous medium and interfacial drag). Steady-state solution with non-zero water volume fraction throughout the bed bulk was interpreted as a stable configuration, and the maximum heat flux at which such a solution existed was referred to as the Dryout Heat Flux (DHF).

Multidimensional configurations of the debris bed were treated either experimentally, or by numerical simulations. So far, axisymmetric porous beds of simple shapes (conical, cylindrical, mound-shaped) received most attention [11, 12]. Generally, it has been established quite well that heap-like configurations are better coolable than a flat porous layer of the same height due to enhanced water ingress into the bed through its side surface in comparison with the counter-current flow (descending water and ascending vapor), characteristic of one-dimensional beds. However, for the same mass of the debris bed, flat configuration provides higher values of the total decay heat that can be removed, than a heap-like configuration [13, 14, 15, 16].

Despite the progress in understanding the behavior and coolability of a heat-releasing bed in a pool, there are still remaining issues which have to be resolved [18, 19], including the uncertainties in the bed properties, shape and system conditions (pressure, subcooling etc.). For non-flat debris beds, computationally expensive numerical simulations are required in order to determine if a debris bed of a certain shape and properties (particle diameter, porosity) is coolable at a particular system pressure and decay heat specific power.

Severe accident risk analysis should include quantification of aleatory (accident scenario-related) and epistemic (modeling) uncertainties inherent in the problem. To this end, large number of simulations is required, which is not feasible with full numerical models. A way forward is the development of surrogate models that approximate, in a computationally inexpensive way, the response surface of a full model with sufficient accuracy [2]. Such models are widely used in engineering as a means facilitating analysis and design of complex systems [20]. Usually a database of the full (detailed and thus computationally expensive) model solutions is necessary in order to develop an approximation (surrogate) model. As the database is often limited, there is a concern about reliability of the surrogate model predictions in the interpolation and (even more so) in extrapolation regime. One way of increasing reliability of the surrogate model is to retain significant part of the basic physics explicitly in the surrogate model, and provide calibrated closures that are applicable for the whole application domain.

In the current work, we consider the coolability problem for a heat-releasing porous bed from the basic physics point of view, in order to derive the functional relationships determining the coolability boundary in the multidimensional parameters space. We then analyze the well-known one-dimensional solutions and propose analytical approximations describing the coolability boundary. The analysis is performed for three drag models, two of which take into account the interfacial drag.

2. PROBLEM FORMULATION

2.1. Dimensional formulation

Consider a general coolability problem for an arbitrary-shaped heat-releasing porous bed submerged in a water pool at saturation conditions. The porous bed has homogeneous properties (d,ε) and constant volumetric heat release rate Q per unit volume of the porous bed (the latter quantity can be related to the specific heating power W, solid material density ρ_s, and porosity ε by $Q=(1-\varepsilon)\rho_s W$). We are looking for a steady state solution in the whole porous bed for superficial velocities and volume fractions of liquid, α_l, and vapor, $\alpha_v=1-\alpha_l$, such that $\alpha_l>0$ everywhere, i.e. there is no dry zone in the bed. In this case, the heat released by solid

material goes to evaporation of liquid coolant, and the volumetric evaporation rate $\Gamma = Q/\Delta H_{ev}$ is constant throughout the porous bed.

The system of equations describing stationary evaporation and two-phase filtration in the porous bed includes the phase continuity and momentum equations, the latter take into account the linear and quadratic terms [21]:

$$\nabla\left(\rho_i \mathbf{j}_i\right) = \Gamma_i \tag{1}$$

$$\nabla P = \rho_i \mathbf{g} - \left(\frac{\mu_i}{K K_{ri}} \mathbf{j}_i + \frac{\rho_i}{\eta \eta_{ri}} \left|\mathbf{j}_i\right| \mathbf{j}_i \right) + \frac{\mathbf{F}_{ij}}{\alpha_i} \tag{2}$$

Hereafter, the subscript $i = l, v$ refers to liquid and vapor phases, respectively. The source terms in the continuity equation (1) are $-\Gamma_l = \Gamma_v = \Gamma$. Equation (2) relates the pressure gradient ∇P to the sum of the gravity term (with $\mathbf{g}$ being the gravity acceleration) and total drag, the terms in the parentheses describe the drag due to the porous medium. The rightmost term in (2) describes the interfacial drag dependent on the relative phase velocity, with $\mathbf{F}_{ij}$ denoting the force exerted to *i*-th phase by *j*-th: $\mathbf{F}_{lv} = -\mathbf{F}_{vl} = \mathbf{F}$ (so that $\mathbf{F}$ is defined as the force exerted to liquid by moving vapor). All phase properties $\left(\rho_i, \mu_i\right)$ are assumed to be constant and correspond to the saturated conditions at the average system pressure P_{sys} (which is the sum of gas space pressure above the pool level, and hydrostatic head in the pool), i.e., effect of variation of pressure inside the bed on the phase properties is neglected, implying $\left|P - P_{sys}\right| \ll P_{sys}$. Note that in Eqs. (1) and (2) the volume fractions of phases $\alpha_v = 1 - \alpha_l = \alpha$ (where α is referred to as the void fraction) are affecting the relative (phasic) permeabilities K_{ri} and passabilities η_{ri}, as well as the interfacial drag $\mathbf{F}$.

We consider a porous bed resting on an impermeable solid boundary (pool bottom), where the superficial velocities of both phases vanish. On the outer boundary of the porous bed, pressure is assumed to follow the hydrostatic pressure distribution in the pool.

For monodisperse spherical particles, the absolute permeability and passability are related to the bed porosity, ε, and particle diameter, *d*, by [21]

$$K = \frac{\varepsilon^3 d^2}{150\left(1-\varepsilon\right)^2}, \qquad \eta = \frac{\varepsilon^3 d}{1.75\left(1-\varepsilon\right)} \tag{3}$$

These relations can also be used for particles of arbitrary shapes and size distributions, provided that d is considered as a properly averaged effective mean particle diameter providing the same drag as the original bed. A number of averaging approaches were proposed, of which the Sauter mean diameter, defined in such a way that the surface-to-volume ratio of polydisperse particle collection is the same as that of equivalent monodisperse particles, is a popular choice. However, other averaging strategies are also possible, for example, based on the equivalency of total drag forces [22].

Spatial distributions are sought for the void fraction α, superficial velocities $\mathbf{j}_i$ of both phases, and pressure P, satisfying the condition $\alpha < 1$ in the porous bed. If for some set of parameters such a solution does not exist, dryout must occur and, thus, the configuration is

considered to be non-coolable. The coolability problem is, thus, reduced to finding the boundary surface in the parameter space separating the domains of existence and non-existence of solutions to equations (1) and (2). Note that this is a conservative assumption, as debris temperatures can be stabilized at relatively moderate levels if the dry zone is relatively small [23, 24].

Before resorting to the analysis of the dryout boundary, note that the form of two-phase momentum equation (3) with scalar permeability and passability (4) is widely used in the literature; however, this form was derived for the most part empirically. An interesting research avenue is development of drag model on more mechanistic grounds, by formal averaging of the local momentum equations of each phase [25–30]. In this approach, tensor quantities appear in the drag laws. Potential extension of the approach presented in this paper to such more complicated governing equations containing a larger number of internal scales and respective closures is a subject of future work.

2.2. Non-dimensional form

The scales of different physical quantities are denoted hereafter by asterisk. We consider a heap-shaped porous bed and take its height for the length scale: $L^* = H$. The density and viscosity scales are taken equal to the corresponding vapor properties, $\rho^* = \rho_v$ and $\mu^* = \mu_v$ (therefore, non-dimensional density and viscosity of vapor are equal to unity), the pressure scale is introduced as $P^* = \rho^* g L^*$, the interfacial drag is normalized by $\rho^* g$.

Three independent characteristic velocities can be formed of the problem parameters:

$$J_1 = \frac{K\rho_v g}{\mu_v}, \qquad J_2 = \sqrt{\eta g}, \qquad J_\Gamma = \frac{\Gamma H}{\rho_v} \tag{4}$$

Of these, J_1 and J_2 are related to the linear and quadratic drag terms in (2), while J_Γ is obtained from the characteristic mass flux of vapor, given the volumetric evaporation rate and porous bed height. Two independent non-dimensional quantities relating these velocities are

$$\chi = \frac{J_1}{J_2} = \frac{K\rho_v g}{\mu_v\sqrt{\eta g}} = \frac{\rho_v (K/\eta)\sqrt{\eta g}}{\mu_v}, \qquad q = \frac{J_\Gamma}{J_2} = \frac{QH}{\Delta H_{ev}\rho_v\sqrt{\eta g}} \tag{5}$$

Parameter χ has the meaning of the Reynolds number based on the characteristic porous medium size K/η, velocity $\sqrt{\eta g}$, density ρ_v, and viscosity μ_v. Parameter q is the non-dimensional heat flux at the top point of the porous bed, QH, normalized by the evaporation heat flux carried along by the vapor moving with the superficial velocity $\sqrt{\eta g}$. Note that definitions (4) and relations (5) contain the quantities K and η entering the drag law (2), rather than individual parameters (d, ε). However, for monodisperse spherical particles (see (3)), these formulas can be expressed in the following form:

$$\chi = 8.8\cdot 10^{-3}\frac{\rho_v d_\varepsilon\sqrt{d_\varepsilon g}}{\mu_v}, \qquad d_\varepsilon = \frac{d\varepsilon}{1-\varepsilon} \tag{6}$$

Evidently, the particle diameter d and porosity ε enter the non-dimensional parameter χ not independently, but as the characteristic pore size d_ε.

Introduce now non-dimensional quantities denoted by tilde using the above scales; the superficial velocities of both phases are normalized by J_Γ. The governing equations (1), (2) take the following form:

$$\tilde{\nabla}\left(\tilde{\mathbf{j}}_l\right) = -\tilde{\rho}_l^{-1} \tag{7}$$

$$\tilde{\nabla}\left(\tilde{\mathbf{j}}_v\right) = 1 \tag{8}$$

$$-\tilde{\nabla}\tilde{P} + \tilde{\mathbf{g}} = \frac{q\chi}{K_{rv}}\tilde{\mathbf{j}}_v + \frac{q^2}{\eta_{rv}}\left|\tilde{\mathbf{j}}_v\right|\tilde{\mathbf{j}}_v + \frac{\tilde{\mathbf{F}}}{\alpha} \tag{9}$$

$$-\tilde{\nabla}\tilde{P} + \tilde{\rho}_l\tilde{\mathbf{g}} = \frac{q\chi\tilde{\mu}_l}{K_{rl}}\tilde{\mathbf{j}}_l + \frac{q^2\tilde{\rho}_l}{\eta_{rl}}\left|\tilde{\mathbf{j}}_l\right|\tilde{\mathbf{j}}_l - \frac{\tilde{\mathbf{F}}}{1-\alpha} \tag{10}$$

where $\tilde{\mathbf{g}} = \mathbf{g}/g$ is the unit vector directed downwards.

Further analysis of equations (7)–(10) requires particular closures for relative phase permeabilities K_{ri}, passabilities η_{ri}, and interfacial drag $\tilde{\mathbf{F}}$. In what follows, we consider first the well-known one-dimensional problem of a top-flooded internally heated particulate bed, with emphasis on the functional form of the dryout condition for different drag models. After that, we extend the results to multidimensional configurations.

3. GENERAL FORM OF DRYOUT CONDITION

3.1. Models without interfacial drag

We begin the analysis of dryout condition by considering a simple case where the relative phase permeabilities K_{ri} and passabilities η_{ri} are functions of the respective volume fractions α_i only, and the interfacial drag is not taken into account. Such models were proposed in [3, 4, 5], with power-law functions

$$\begin{matrix} K_{rl} = (1-\alpha)^n, & \eta_{rl} = (1-\alpha)^m \\ K_{rv} = \alpha^n, & \eta_{rv} = \alpha^m \end{matrix}, \qquad \mathbf{F} = 0 \tag{11}$$

All three models mentioned have the exponents $n = 3$ in the relative permeabilities, whereas the exponents in the relative passabilities are $m = 4$ [3], $m = 5$ [4], and $m = 6$ [5]. The value $m = 5$ proposed by Reed [4] seems to give the best agreement with experiments and will be used hereafter.

Since no additional dimensional parameters are introduced in the models (11), it follows from equations (7)–(10) that for two geometrically similar porous beds, non-dimensional solutions for α, $\tilde{\mathbf{j}}_l$, and $\tilde{\mathbf{j}}_v$ are the same, provided that four non-dimensional parameters, q, χ, $\tilde{\rho}_l$, and $\tilde{\mu}_l$ coincide. This means that the surface in the parameter space, bounding the domain where steady-state solutions exist, can be expressed as a relationship between these four parameters, or one of them can be expressed as a function of the other three. It is convenient to consider χ, $\tilde{\rho}_l$, and $\tilde{\mu}_l$ as independent parameters, and determine the boundary value corresponding to occurrence of dryout for the non-dimensional heat flux at the top point of the porous bed q. In accordance with the traditional notation in coolability studies, we call the corresponding dimensional quantity the Dryout Heat Flux (DHF), and denote its non-dimensional value by q_{DHF}. Therefore,

$$q_{\mathrm{DHF}} = \Phi\left(\chi, \tilde{\rho}_l, \tilde{\mu}_l\right) \tag{12}$$

It should be noted that the first parameter involves the drag characteristics of the porous medium, whereas the second and third ones depend solely on the physical properties of the coolant. Recall now that we assume that the coolant in the heat-releasing porous medium is at saturation conditions, in which case all coolant properties (including density and viscosity of both liquid and vapor phases) are single-valued functions of local pressure, or, under the assumption of small pressure deviations with respect to the prevailing system pressure P_{sys}, all properties are determined by P_{sys} only. If we consider P_{sys} as a non-dimensional quantity (for example, by measuring the system pressure in bars) the relationship (12) can be presented in the following form:

$$q_{\mathrm{DHF}} = \Phi\left(\chi, P_{sys}\right) \tag{13}$$

The above analysis shows the functional dependence of dryout heat flux on the problem parameters. However, the function Φ in (13) is specific to porous bed geometry, it cannot be found without solving equations (7)–(10), either analytically (where possible) or numerically. A straightforward way to obtain Φ for some particular porous bed shape would be to carry out large enough number of simulations and approximate the response surface by any suitable fitting technique. We, however, attempt to use as much available knowledge as possible, before resorting to the response surface fitting. To this end, we apply the asymptotic interpolation method [33] which uses the known two-sided asymptotic behavior of the solution at the left and right ends of the interval, and aims at finding an interpolant satisfying asymptotic behaviors at both ends.

It is known that porous bed coolability is improved when particle size or porosity are increased because of lower drag and, thus, easier vapor evacuation from the porous material. Therefore, for any system pressure P_{sys} the function Φ is increasing monotonically with χ, with the following asymptotic behavior:

1. $\chi \to 0$. This case corresponds to low permeability K and large passability η, and thus, to the linear drag terms being dominant over the quadratic terms in (9) and (10). In this limit, q_{DHF} must be independent of η and depend only on K, which means that the ratio Φ/χ must be finite, or

$$\Phi \to \chi \cdot \Phi_0\left(P_{sys}\right) \tag{14}$$

2. $\chi \to \infty$. This case corresponds to high permeability K and low passability η, and thus, to the quadratic drag terms being dominant over the linear terms in (9) and (10). In this limit, q_{DHF} must become independent of K and depend only on η, which means that function Φ must tend to a finite value:

$$\Phi \to \Phi_\infty\left(P_{sys}\right) \tag{15}$$

Importantly, the asymptotic functions Φ_0 and Φ_∞ are independent of the porous medium properties, but depend on the system pressure P_{sys} only. Following [14, 16], we rescale the argument χ and function Φ by Φ_0 and Φ_∞:

$$\hat{\chi} = \chi \frac{\Phi_0}{\Phi_\infty}, \qquad \hat{\Phi} = \frac{\Phi}{\Phi_\infty} \tag{16}$$

in such a way that the resulting function $\hat{\Phi}\left(\hat{\chi}, P_{sys}\right)$ would possess at any pressure P_{sys} the following properties:

$$\left.\frac{d\hat{\Phi}}{d\hat{\chi}}\right|_{\hat{\chi}=0} = 1, \qquad \lim_{\hat{\chi}\to\infty} \hat{\Phi} = 1 \tag{17}$$

The function $\hat{\Phi}$ introduced in (16) still formally depends on both $\hat{\chi}$ and P_{sys} defining a family of functions $\hat{\Phi}\left(\hat{\chi}\right)$ depending parametrically on P_{sys}. Since the asymptotic behavior of $\hat{\Phi}$ at $\hat{\chi} \to 0$ and "at infinity", described by (17), is independent of P_{sys}, one can expect that the influence of system pressure on the dryout heat flux manifests itself mainly through the two single-argument functions, $\Phi_0\left(P_{sys}\right)$ and $\Phi_\infty\left(P_{sys}\right)$, see (14) and (15), and that the family of curves $\hat{\Phi}\left(\hat{\chi}, P_{sys}\right)$ is condensed tightly around a function of single variable $\hat{\Phi}\left(\hat{\chi}\right)$. Should this hypothesis hold true, the whole dependence of dryout heat flux on problem parameters (12) can be described by three single-argument functions, $\Phi_0\left(P_{sys}\right)$, $\Phi_\infty\left(P_{sys}\right)$, and $\hat{\Phi}\left(\hat{\chi}\right)$, for which appropriate approximations can be found easily, providing a computationally inexpensive surrogate model for the dryout boundary. The accuracy of this hypothesis, however, cannot be known beforehand and must be checked by comparing predictions of the surrogate model with the "raw" results of complete model, as will be demonstrated in the following sections.

3.2. Models with explicit interfacial drag

The same analysis can be applied to models that take into account the drag due to relative motion of liquid and vapor phases in the pores (interfacial drag). The possibility of finding similarity solutions, however, depends on whether the interfacial drag force $\tilde{\mathbf{F}}$ obeys the same scaling as the drag of flowing phases due to interaction with solid particles. We consider here two such models available in the literature, paying most attention to the functional form of the closures for the relative permeabilities and passabilities, and for the drag force.

3.2.1. Drag model by Schulenberg and Müller [6]

Schulenberg and Müller derived the interfacial drag model [6] by considering the main scales present in the porous medium and considering coarse particles for which the capillary forces due to particle wettability can be neglected, with all acting forces scaled with the buoyancy force. The resulting expressions determining the two-phase drag are

$$\begin{aligned} &K_{rl} = (1-\alpha)^3, \quad \eta_{rl} = (1-\alpha)^5 \\ &K_{rv} = \alpha^3, \qquad \eta_{rv} = \begin{cases} \alpha^6, & \alpha > \alpha_* \approx 0.316, \\ 0.1\alpha^4 & \alpha \le \alpha_* \end{cases} \end{aligned} \tag{18}$$

$$\mathbf{F} = 350\alpha(1-\alpha)^7(\rho_l - \rho_v) g \frac{\rho_l K}{\eta\sigma} |\mathbf{V}_r| \mathbf{V}_r, \qquad \mathbf{V}_r = \frac{\mathbf{j}_v}{\alpha} - \frac{\mathbf{j}_l}{1-\alpha} \tag{19}$$

Note that the relative permeabilities and passabilities (18) are functions of void fraction α only (as was the case in Section 3.1). Consider the possibility of using similarity approach for the

interfacial drag $\mathbf{F}$. Reducing (19) to non-dimensional form with the scales introduced in Section 2.2, we obtain

$$\tilde{\mathbf{F}} = 350\alpha\left(1-\alpha\right)^7 \frac{\left(\tilde{\rho}_l - 1\right)\tilde{\rho}_l}{\tilde{\mu}_l} \mathrm{Ca}\cdot q^2 \left|\tilde{\mathbf{V}}_r\right| \tilde{\mathbf{V}}_r, \qquad \tilde{\mathbf{V}}_r = \frac{\tilde{\mathbf{j}}_v}{\alpha} - \frac{\tilde{\mathbf{j}}_l}{1-\alpha} \tag{20}$$

with $\mathrm{Ca} = J_1\mu_l / \sigma$ being the capillary number based on the characteristic velocity J_1. With the same reasoning as in derivation of Eq. (13), we conclude that the dryout boundary can be represented by

$$q_{\mathrm{DHF}} = \Phi\left(\chi, P_{sys}, \mathrm{Ca}\right) \tag{21}$$

Asymptotic behavior of (21) at small and large χ can be represented by two functions Φ_0 and Φ_∞ (see (14), (15)) which, however, depend on two variables, P_{sys} and Ca .

3.2.2. Tung and Dhir Original and Modified Models [7, 8]

The second model explicitly taking into account the interfacial drag considered here was originally proposed by Tung and Dhir [7] and later modified and validated by Schmidt et al [8].

In the original model [7], the following relationships describe the gas-particle drag:

- $0 \le \alpha \le \alpha_3$ (bubbly and slug flow):

$$K_{rv} = \left(\frac{1-\varepsilon}{1-\varepsilon\alpha}\right)^{4/3} \alpha^4, \quad \eta_{rv} = \left(\frac{1-\varepsilon}{1-\varepsilon\alpha}\right)^{2/3} \alpha^4 \tag{22}$$

- $\alpha_3 \le \alpha \le \alpha_4$ (transition)
- $\alpha_4 \le \alpha \le 1$ (pure annular flow):

$$K_{rv} = \left(\frac{1-\varepsilon}{1-\varepsilon\alpha}\right)^{4/3} \alpha^3, \quad \eta_{rv} = \left(\frac{1-\varepsilon}{1-\varepsilon\alpha}\right)^{2/3} \alpha^3 \tag{23}$$

The boundaries between different flow regimes are

$$\begin{aligned} &\alpha_1 = \min(0.3,\, 0.6(1-\gamma)^2), \quad \gamma = \frac{D_b}{d} \\ &\alpha_2 = \frac{\pi}{6} \approx 0.52, \quad \alpha_3 = 0.6, \quad \alpha_4 = \frac{\pi\sqrt{2}}{6} \approx 0.74 \end{aligned} \tag{24}$$

The liquid drag due to interaction with the porous medium particles is described by the relative phase permeability and passability

$$K_{rl} = \eta_{rl} = \left(1-\alpha\right)^4. \tag{25}$$

The interfacial drag is

$$\mathbf{F} = \varepsilon C_1 \frac{\mu_l}{D_b^2}\left(1-\alpha\right)\mathbf{V}_r + C_2 \frac{\left(1-\alpha\right)\rho_l + \alpha\rho_v}{D_b}\left(1-\alpha\right)^2 \left|\mathbf{V}_r\right| \mathbf{V}_r \tag{26}$$

where $\mathbf{V}_r = \mathbf{j}_v / \alpha - \mathbf{j}_l / (1-\alpha)$ is the relative phase velocity. The bubble diameter used in the above relations for the porous medium drag is

$$D_b = 1.35\sqrt{\frac{\sigma}{g\left(\rho_l - \rho_v\right)}} \tag{27}$$

The friction coefficients are given separately for bubbly and slug flow:

- $0 \le \alpha \le \alpha_1$ (bubbly flow):

$$C_1 = 18\alpha\,,\; C_2 = 0.34\left(1-\alpha\right)^3\alpha \tag{28}$$

- $\alpha_2 \le \alpha \le \alpha_3$: (slug flow)

$$C_1 = 5.21\alpha\,,\; C_2 = 0.92\left(1-\alpha\right)^3\alpha \tag{29}$$

For high void fractions, $\alpha_4 \le \alpha \le 1$ the drag is obtained from

$$\mathbf{F} = \frac{\mu_v}{KK_{rv}}\left(1-\alpha\right)\mathbf{V}_r + \left(1-\alpha\right)\alpha\frac{\rho_v}{\eta\eta_{rv}}\left|\mathbf{V}_r\right|\mathbf{V}_r \tag{30}$$

Smooth transition between flow regimes is obtained by third-order polynomial interpolation.

The modifications to the drag model [7] introduced and validated by Schmidt *et al.* [8] include i) limiting the bubble diameter (27), ii) changing the flow regime boundaries (24), and iii) changing the interfacial drag (30) for particles smaller than 6-8 mm. The corresponding modified values denoted by superscript m are:

$$\begin{aligned}
D_b^m &= \min\left(D_b, 0.41d\right)\\
\alpha_{1-3}^m &= \alpha_{1-3} + \min\left(\frac{\pi/6}{5}\left(d-8\,\text{mm}\right), 0\right),\\
\alpha_4^m &= \alpha_4 + \min\left(\frac{\pi/6}{5}\left(d-6\,\text{mm}\right), 0\right),\\
\mathbf{F}^m &= \mathbf{F}\cdot\left(1-\alpha\right)^2\cdot\min\left(\left(\frac{d}{6\,\text{mm}}\right)^2, 1\right)
\end{aligned} \tag{31}$$

(in the bottom three lines, d is measured in millimeters).

From the similarity point of view, one can see that relative permeabilities and passabilities of gas phase (22) and (23) are expressed as powers of the void fraction α multiplied by a factor in parentheses containing the porosity ε. On the other hand, the flow regime boundaries (24) and (31) contain the particle diameter d. There are also a number of additional dimensional parameters appearing in the drag law formulation, including the bubble diameter (27) and the particle sizes 6 and 8 mm in the modification (31). The non-dimensional form of interfacial drag (26) is expressed by

$$\tilde{\mathbf{F}} = \varepsilon C_1\frac{\text{Ca}}{1.35^2}\left(\tilde{\rho}_l - 1\right)\left(1-\alpha\right)q\chi\tilde{\mathbf{V}}_r + C_2\text{Fr}\left(\left(1-\alpha\right)\tilde{\rho}_l + \alpha\right)\left(1-\alpha\right)^2 q^2\chi^2\left|\tilde{\mathbf{V}}_r\right|\tilde{\mathbf{V}}_r \tag{32}$$

where $\text{Ca} = J_1\mu_l/\sigma$ is the capillary number, $\text{Fr} = J_1^2/gD_b$ is the Froude number based on the superficial velocity J_1 and characteristic bubble ascend velocity $\sqrt{gD_b}$ due to buoyancy. The interfacial drag in the annular regime (30) takes the following non-dimensional form:

$$\tilde{\mathbf{F}} = \frac{q\chi}{K_{rv}}\left(1-\alpha\right)\tilde{\mathbf{V}}_r + \left(1-\alpha\right)\alpha\frac{q^2}{\eta_{rv}}\left|\tilde{\mathbf{V}}_r\right|\tilde{\mathbf{V}}_r \tag{33}$$

Overall, the dryout boundary corresponding to DHF can be written, by analogy with (13), as

$$q_{\text{DHF}} = \Phi\left(\chi, P_{sys}, \text{Ca}, \text{Fr}, \frac{d}{D_b}, \frac{d}{1\,\text{mm}}\right) \tag{34}$$

where the latter parameter appears due to modifications (31) involving the dimensional particle diameter measured in millimeters.

Evidently, larger number of parameters appearing in the functional dependency of non-dimensional dryout heat flux in (21) and (34) makes the asymptotic interpolation, originally proposed in Section 3.1 for a model without interfacial drag, more complicated. However, it will be shown in the next section that such an interpolation can be performed approximately, with the accuracy sufficient for engineering estimates of dryout conditions.

4. DRYOUT HEAT FLUX FOR ONE-DIMENSIONAL TOP-FLOODED POROUS BED

4.1. Solution Procedure

Dryout in a one-dimensional internally heated porous bed resting on an impermeable base with water supplied on its top (a top-flooded bed) has been studied in many experimental and analytical works [3, 4, 5, 6, 7, 8, 9, 12, 18], including those where the drag models quoted in Section 2 were derived and validated. The procedure for finding the dryout conditions can be summarized as follows (see details, e.g. in [6]). In the one-dimensional top-fed configuration, vapor is flowing upwards and replacing it water is flowing downwards, creating so-called counter-current flow regime, with the highest (by absolute value) superficial velocities of vapor and liquid reached at the bed top. In the steady state, these velocities, as it follows from integration of continuity equations (1), are $j_v^{top} = QH / \rho_v \Delta H_{ev}$, $j_l^{top} = -j_v^{top} \left(\rho_v / \rho_l \right)$. Substituting these into the momentum equations (2) and eliminating the pressure gradient, we arrive at a single quadratic equation with respect to j_v^{top}, with the coefficients expressed in terms of the void fraction at the bed top, α^{top}, and containing other problem parameters involved in the drag laws and depending on the particular drag model. The largest possible solution $j_v^{top} = j_v^{\max}$ to the quadratic equation determines the dryout heat flux $\mathrm{DHF} = j_v^{\max} \rho_v \Delta H_{ev}$.

Due to complexity of the coefficients of the quadratic equation (especially when the interfacial drag is included in the model), determination of DHF requires numerical solution of a non-linear algebraic equation with respect to the void fraction α^{top}. Thus, even in the one-dimensional case the problem of finding DHF and analyzing its dependence on properties of porous material and system pressure does not have a simple analytical solution. It becomes a much more computationally expensive task for multi-dimensional configurations.

In this work, we develop a computationally efficient surrogate model, which can be used for different problem statements. To demonstrate the approach, we consider the 1D case and calculate DHF for a sufficiently large number of cases, varying each input parameter in the range of interest for the particular physical problem. Then we analyze the database of solutions obtained using the general functional form of dryout criterion derived in Section 3, consider the limiting cases and perform asymptotic interpolation between them. The purpose is to derive simple enough approximations while retaining the key physics of the exact solution. We then evaluate the deviation of the approximate solution arising due to the presence of additional parameters in the multi-parameter functional form, not taken into account directly in the primary approximation. After that, we discuss extension of this approach to other bed configurations.

As the particular problem, consider coolability of a heat-releasing porous bed in a water pool under the conditions relevant to severe accidents in light water nuclear power plant reactors. The parameter ranges are summarized in Table 1, their choice was based on the following

grounds. The range of particle diameter $d = 0.5 - 25$ mm was taken wider than the expected particle sizes typical of molten corium-water interaction (the upper limit for the porous particle size can hardly exceed 10 mm, see the fuel-coolant interaction experiments FARO [31] and DEFOR [32]). A wider range was taken in order to obtain large enough values of argument χ necessary to study the asymptotic behavior of the function describing the dryout heat flux. The porosity range was based on the experimental data from different tests [17, 18, 19], while the system pressure range covers possible values of nuclear reactor containment pressure in severe accident conditions [2].

Table 1 Parameter ranges

Parameter	Description	Range
d	Mean particle diameter, [mm]	0.5–25
ε	Porosity, [–]	0.3–0.55
P_{sys}	Average pressure in the porous bed, [bar]	1–5

In the calculations, the model input parameters were entered in the dimensional form. Particle diameter was varied with the step 0.2 mm (123 values), porosity with the step 0.025 (11 values), system pressure with the step 0.2 bar (21 value), with the number of cases totaling to 28413 for a given drag model. For each combination $\left(d, \varepsilon, P_{sys}\right)$, water and vapor properties on the saturation line $\left(\rho_l, \rho_v, \mu_l, \mu_v, \Delta H_{ev}, \sigma\right)$ were calculated at the current pressure P_{sys} according to the IAPWS-IF97 formulation [34]; the absolute permeabilities and passabilities were obtained from the formulas (3) as functions of current particle diameter d and porosity ε. After that, the dimensional dryout heat flux DHF was calculated by the procedure outlined above. The non-dimensional drag parameter χ was then evaluated from (5), and the non-dimensional dryout heat flux calculated as $q_{\mathrm{DHF}} = \mathrm{DHF} / \left(\Delta H_{ev} \rho_v \sqrt{\eta g}\right)$, providing a single point on the $\left(\chi, q_{\mathrm{DHF}}\right)$ plane. The database of all calculated points was then analyzed in order to find the best fit to the response surface. In the following sections, results obtained for the three drag models are presented.

4.2. Results

4.2.1. Drag model by Reed [*4*]

Consider first the simplest case where interfacial drag is not taken into account. It was shown in Section 3.1 that the non-dimensional dryout heat flux q_{DHF} depends on two parameters, χ and P_{sys}, see (13). This means that, for a fixed pressure P_{sys}, all results obtained for different particle diameters d and porosity ε must be described by a function of single variable χ. This is confirmed in Fig. 1a where $q_{\mathrm{DHF}} = \Phi\left(\chi, P_{sys}\right)$ is plotted, each dot corresponding to a single combination of parameters from Table 1 (for clarity, only some indicated pressures are represented). Dots are packed quite tightly and look like continuous curves, confirming that χ is a proper argument of the dependence.

The functions Φ_0 and Φ_∞ describing the asymptotic behavior at small and large χ (see (14) and (15)) were determined from the data obtained, they are presented in Fig. 1b by the filled

and open dots, respectively. To facilitate their practical use, the following approximating formulas were found:

$$\Phi_0 = \frac{1000}{0.295 + 1.78 P_{sys}^{1.2}} \tag{35}$$

$$\Phi_\infty = \frac{100}{1 + 4.386 P_{sys}^{0.67}} \tag{36}$$

Functions (35) and (36) are plotted in Fig. 1b by solid lines.

With the use of functions Φ_0 and Φ_∞, all data presented in Fig. 1a were transformed to the form (16). The results are presented in Fig. 1c, with the asymptotic behavior (17) shown by the dashed lines. One can see that for Reed's drag model (and, accordingly, for all models belonging to family (11)) the asymptotic interpolation provides a unified description of the dryout heat flux. For the function $\hat{\Phi}(\hat{\chi})$ presented in Fig. 1c, the following approximation was found:

$$\hat{\Phi} = \frac{\bar{\chi}}{1 + \bar{\chi}}, \qquad \bar{\chi} = \left(\frac{\hat{\chi}}{0.675} \right)^{1.12} \tag{37}$$

In Fig. 1d, all points from Fig. 1a,c are replotted against the transformed abscissa $\chi' = \bar{\chi} / (1 + \bar{\chi})$ spanning the range $[0,1]$; the diagonal straight line represents the approximation (37) taking a simple form $\hat{\Phi} = \chi'$. Agreement between the actual points and approximation (37) is within 1%, which is quite sufficient for the engineering purposes given typical magnitude of uncertainty due to the possible ranges of the input parameters.

Thus, we have shown that for Reed's drag model [4] for a flat porous bed the dependence of dryout heat flux on all problem parameters can be expressed in the non-dimensional form by three single-argument functions $\Phi_0(P_{sys})$, $\Phi_\infty(P_{sys})$, and $\hat{\Phi}(\hat{\chi})$. Approximations to all these functions (35)–(37) provide a convenient and computationally efficient way to evaluate the dryout conditions without the need to solve numerically any equations.

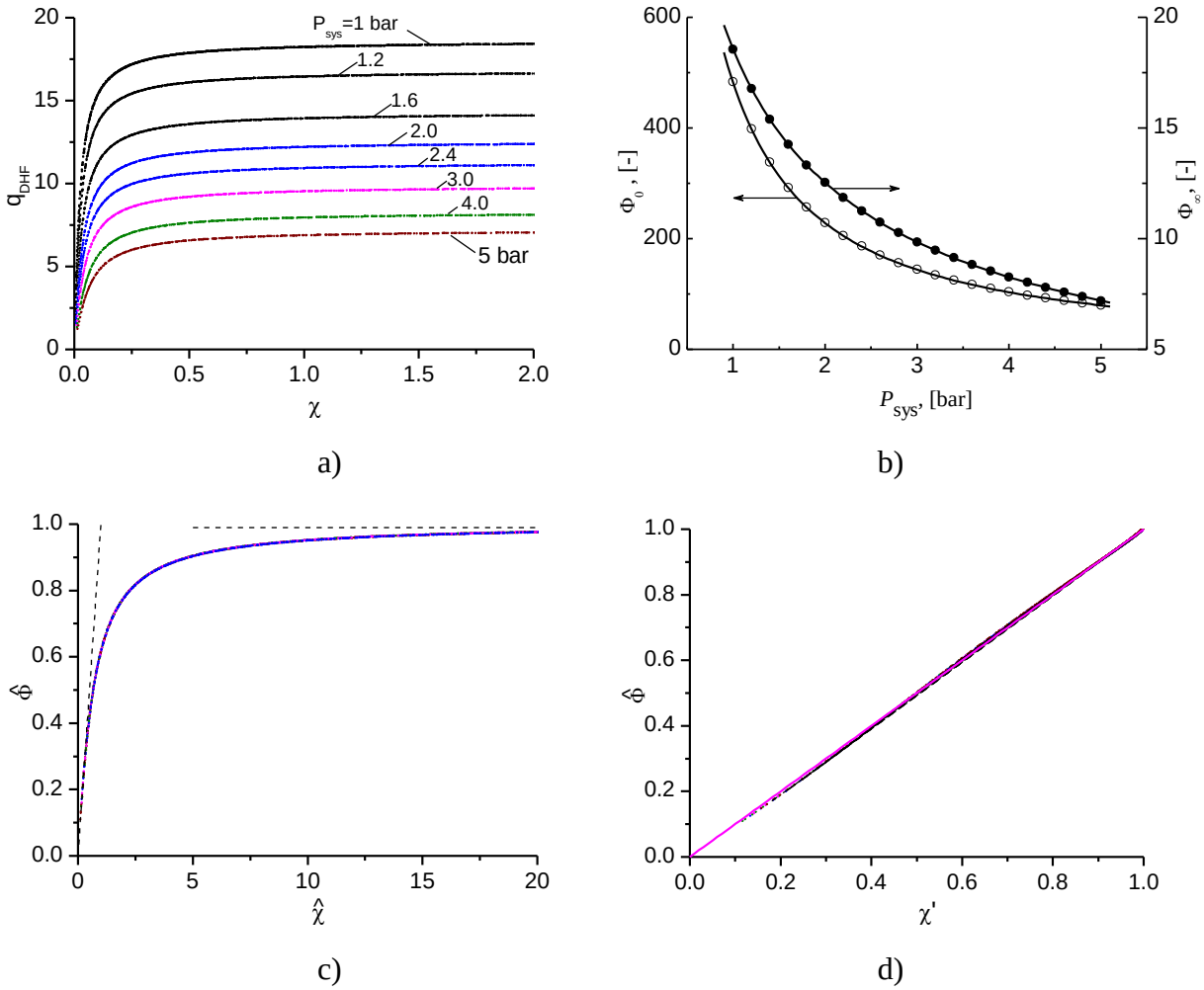

Fig. 1. Dryout heat flux in non-dimensional variables for a flat porous bed (Reed's drag model [4]): a) dependence $q_{\mathrm{DHF}}\left(\chi, P_{sys}\right)$, b) functions $\Phi_0\left(P_{sys}\right)$ and $\Phi_\infty\left(P_{sys}\right)$ describing asymptotic behavior at $\chi \to 0$ and $\chi \to \infty$, c) data in transformed variables $\hat{\Phi}\left(\hat{\chi}\right)$, d) approximation $\hat{\Phi}\left(\chi'\right)$ by (37).

4.2.2. Drag model by Schulenberg and Müller [6]

Similarity analysis carried out in Section 3.2.1 shows that for the model by Schulenberg and Müller [6], which explicitly takes into account the interfacial drag, non-dimensional dryout heat flux depends not only on the two primary parameters χ and P_{sys}, but also on an additional parameter Ca (capillary number) involving surface tension, see (21). Therefore, as was discussed above, the functions Φ_0 and Φ_∞ describing the asymptotic behavior of $q_{\mathrm{DHF}} = \Phi\left(\chi, P_{sys}, \mathrm{Ca}\right)$ at small and large χ depend on two parameters P_{sys} and Ca. However, it would be highly beneficial to represent the multidimensional response surface by a number of one-dimensional functions. In what follows, we analyze the results obtained in the parameter ranges from Table 1 from this point of view.

In Fig. 2a, the non-dimensional dryout heat flux q_{DHF} is plotted against the parameter χ for a number of fixed values of system pressure P_{sys}. Two main differences can be observed in comparison with the corresponding curves in Fig. 1,a (Reed's model). Firstly, there is some scatter of points for a fixed pressure, more visible at low pressures; this scatter reflects the effect of parameter Ca. Secondly, the general behavior of the data for each pressure is non-monotonic: as χ increases, q_{DHF} is growing to reach some maximum, after which it decreases gradually. Note that this decrease is not visible in Fig. 2,a at high pressures, however, the range of χ presented in the graph is smaller than the overall range spanned by all combinations of problem parameters in Table 1. Notably, the scatter of points becomes more significant after the maximum of q_{DHF} was passed. Recall that high values of χ, as it follows from Eq. (6), correspond to large particle diameters and high porosity, i.e., they are relevant to very permeable porous beds with high DHF, which are usually not of risk significance [13, 15]. From the point of view of nuclear safety, the most interesting is the other end of the problem parameter spectrum, when porous bed possesses relatively low filtration capacity and is prone to dryout at low heating power. This is achieved at low values of χ, where monotonic increase of q_{DHF} with χ is observed.

Note that in the latter parameter range, scatter of points due to the effect of Ca is low or moderate. For 1D problem with counter-current vapor and water flow, the critical conditions for water ingress are attained at the top boundary where the volume fraction of vapor α takes its maximum value. Accordingly, the volume fraction of water, entering the interfacial drag (19) as $(1-\alpha)^7$, diminishes the magnitude of interfacial drag, and, thus, reduces its relative influence on the dryout conditions.

In order to apply the approach, which proved to be successful in Section 4.2.1, we determine the function Φ_∞ for each pressure not at $\chi \to \infty$, but take the maximum value of q_{DHF} for each dataset corresponding to a given pressure P_{sys}. The highest value of q_{DHF} / χ (corresponding to the smallest particle size and lowest porosity) was taken as the value of Φ_0 for each pressure. The results are presented in Fig. 2,b by dots, with the following best-fit approximations shown by corresponding solid curves (the functional form of the approximations was taken the same as in (35) and (36):

$$\Phi_0 = \frac{1000}{0.261 + 1.84 P_{sys}^{1.2}} \tag{38}$$

$$\Phi_\infty = \frac{100}{1.35 + 5.1 P_{sys}^{0.67}} \tag{39}$$

In Fig. 2,c, the data of Fig. 2,a are replotted in the scaled variables (16), with the dashed lines representing the asymptotic formulas (17). Finally, an approximation formula

$$\hat{\Phi} = \frac{\bar{\chi}}{1+\bar{\chi}}, \qquad \bar{\chi} = \left(\frac{\hat{\chi}}{0.65} \right)^{1.32} \tag{40}$$

was obtained by least-square fitting the data in Fig. 2,c. all points from Fig. 2,a,c are replotted against the transformed abscissa $\chi' = \bar{\chi}/(1+\bar{\chi})$ spanning the range $[0,1]$; the diagonal straight line represents the approximation (40) taking a simple form $\hat{\Phi} = \chi'$. Overall, data deviation from the approximating straight line is within 5%, not counting the differences near the right end of the interval which is not too important from the point of view of applications for which the approximations are derived (very high permeability).

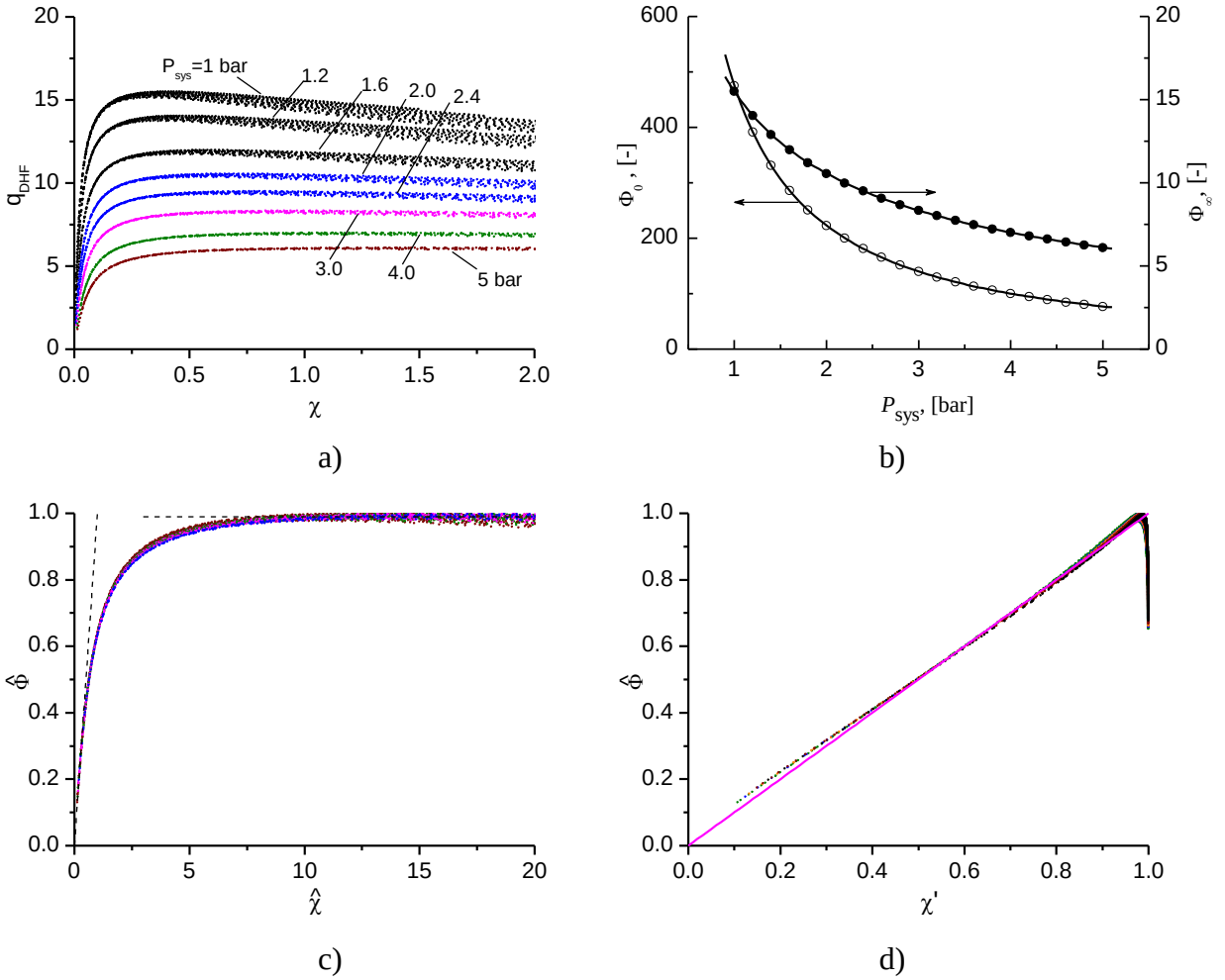

Fig. 2. Dryout heat flux in non-dimensional variables for a flat porous bed (Schulenberg and Müller's drag model [6]): a) dependence $q_{\mathrm{DHF}}(\chi, P_{sys})$, b) functions $\Phi_0(P_{sys})$ and $\Phi_\infty(P_{sys})$ describing asymptotic behavior at $\chi \to 0$ and $\chi \to \infty$, c) data in transformed variables $\hat{\Phi}(\hat{\chi})$, d) approximation $\hat{\Phi}(\chi')$ by (37).

4.2.3. Modified Tung and Dhir's model [7, 8]

Analysis of this model from the similarity point of view performed in Section 3.2.2 shows that the non-dimensional dryout heat flux q_{DHF} is a function of multiple parameters, see (34). However, we attempt here to obtain a small number of one-dimensional functions representing the response surface of the model with accuracy sufficient for engineering applications.

In Fig. 3a, the non-dimensional dryout heat flux q_{DHF} is plotted against the parameter χ for a number of fixed values of system pressure P_{sys}. As was the case in Section 4.2.2, the data

are scattered due to the effect of the remaining parameters in (34). In this model, however, all dependencies are monotonic, similar to the case of Reed's model (Fig. 1a). By the same procedure as in the previous two cases, the asymptotic functions are found, see Fig. 3b:

$$\Phi_0 = \frac{1000}{0.417 + 2.83 P_{sys}^{1.2}} \tag{41}$$

$$\Phi_\infty = \frac{100}{0.83 + 3.3 P_{sys}^{0.65}} \tag{42}$$

After that, the data of Fig. 3a are replotted in a unified manner in Fig. 3c for which the approximating function found is

$$\hat{\Phi} = \frac{\bar{\chi}}{1+\bar{\chi}}, \qquad \bar{\chi} = \left(\frac{\hat{\chi}}{0.825} \right)^{0.965} \tag{43}$$

Finally, all data points are replotted against the transformed abscissa $\chi' = \tilde{\chi} / (1 + \tilde{\chi})$ spanning the range $[0,1]$; the diagonal straight line represents the approximation (43) taking a simple form $\hat{\Phi} = \chi'$. Overall, data deviation from the approximating straight line is within $\pm 7\%$.

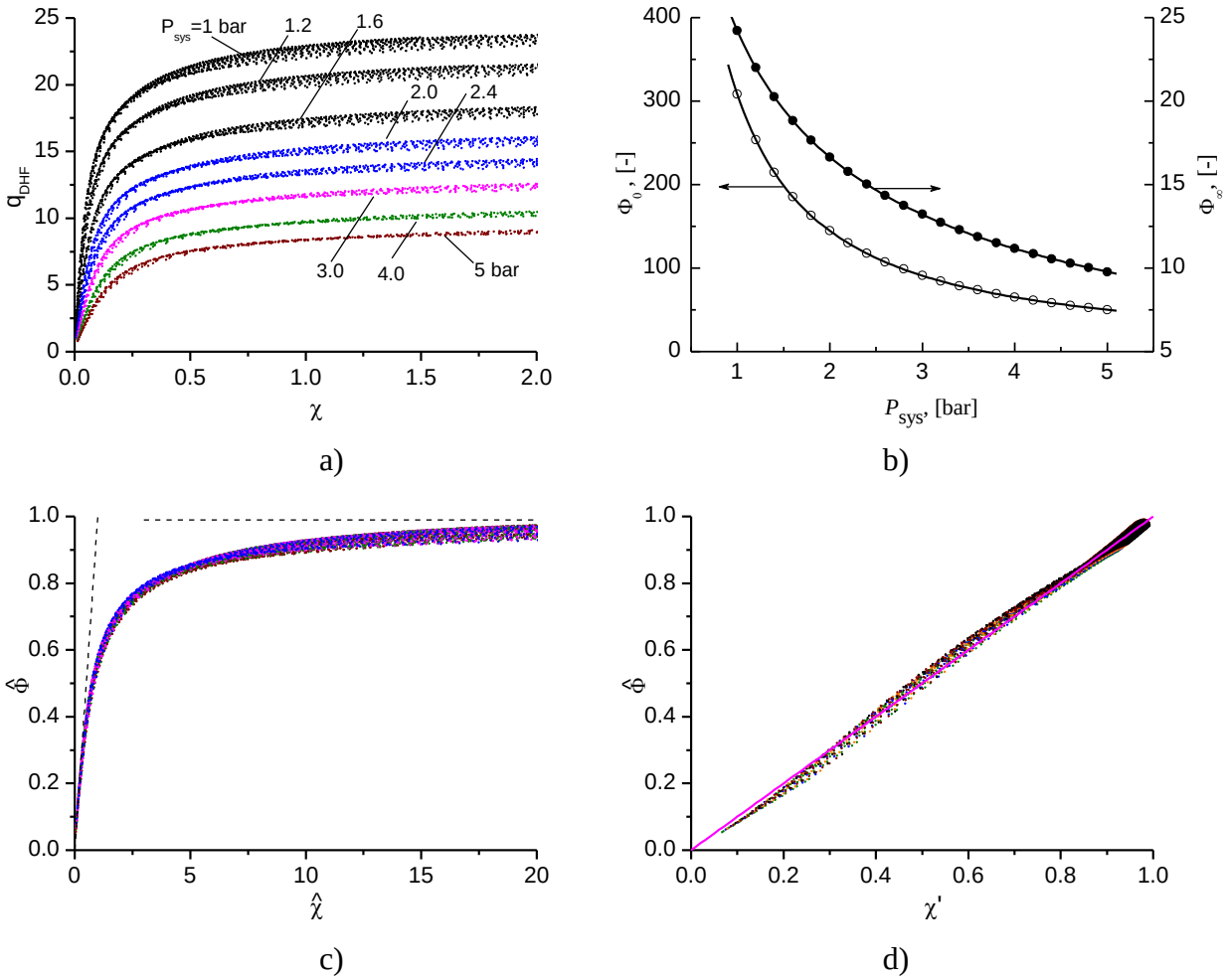

Fig. 3. Dryout heat flux in non-dimensional variables for a flat porous bed (Modified Tung and Dhir's model [7, 8]): a) dependence $q_{\mathrm{DHF}}(\chi, P_{sys})$, b) functions $\Phi_0(P_{sys})$ and $\Phi_\infty(P_{sys})$ describing asymptotic behavior at $\chi \to 0$ and $\chi \to \infty$, c) data in transformed variables $\hat{\Phi}(\hat{\chi})$, d) approximation $\hat{\Phi}(\chi')$ by (37).

4.3. Surrogate Model Implementation

The results presented above provide an efficient way to evaluate the non-dimensional dryout heat flux for a top-flooded internally heated porous bed. With the accuracy acceptable for engineering applications and safety analysis, DHF can be approximated by the set of three one-dimensional functions, albeit with constants dependent on the drag model. For reference, we summarize here the final formulas:

$$\mathrm{DHF} = \Delta H_{ev}\rho_v\sqrt{\eta g}\cdot q_{\mathrm{DHF}} \tag{44}$$

$$q_{\mathrm{DHF}} = \Phi_\infty \frac{\bar{\chi}}{1+\bar{\chi}} \qquad \bar{\chi} = \left(\frac{\hat{\chi}}{\chi_0}\right)^{c_\chi} \tag{45}$$

$$\hat{\chi} = \frac{\rho_v (K/\eta)\sqrt{\eta g}}{\mu_v}\frac{\Phi_0}{\Phi_\infty} \tag{46}$$

$$\Phi_0 = \frac{a_0}{b_0 + c_0 P_{sys}^{d_0}}, \qquad \Phi_\infty = \frac{a_\infty}{b_\infty + c_\infty P_{sys}^{d_\infty}} \tag{47}$$

In Table 2, the constants involved in these correlations are given for the three drag models considered.

Table 2 Constants in correlations (44)–(47)

Drag model	a_0	b_0	c_0	d_0	a_∞	b_∞	c_∞	d_∞	χ_0	c_χ	Rel. error
Reed [4]	1000	0.295	1.78	1.2	100	1.00	4.386	0.67	0.675	1.12	<1%
Schulenberg and Müller [6]	1000	0.261	1.84	1.2	100	1.35	5.1	0.67	0.650	1.32	±4%
Tung and Dhir (modified) [7, 8]	1000	0.417	2.83	1.2	100	0.83	3.3	0.65	0.825	0.965	±7%

It can be seen from (44)–(47) that the dimensional dryout heat flux involves in (44), (46) the water properties on the saturation line (heat of evaporation ΔH_{ev}, vapor density ρ_v and viscosity μ_v) corresponding to the system pressure P_{sys}. Thus, the effect of system pressure on DHF is manifested not only explicitly via the functions Φ_0 and Φ_∞ (see (47)), but also via the coolant properties. In the implementation of surrogate model (44)–(47), it might be convenient to evaluate the saturated water and vapor properties from simpler fitting functions, rather than from quite complicated IAPWS formulation [34]. The following formulas were found to give acceptable accuracy (within 1%) in the range of system pressures $P_{sys} = 1-10$ bar relevant to ex-vessel severe accident problems:

$$
\begin{aligned}
T_s &= 373 + 26.862 \ln P_{sys} + 3.406 \left(\ln P_{sys} \right)^2 \\
\rho_v \left(P_{sys} \right) &= 7.549 \cdot 10^{-2} + 0.531 P_{sys} - 2.43 \cdot 10^{-3} P_{sys}^2 \\
\mu_v \left(T_s \right) &= 1.143 \cdot 10^{-5} \left(\frac{T_s}{350} \right)^{3/2} \frac{350 + 500}{T_s + 500} \\
\rho_l \left(T_s \right) &= 10^3 \cdot \left(1.258 - 1.908 \cdot 10^{-3} T_s + 3.5745 \cdot 10^{-6} T_s^2 \right)^{-1} \\
\mu_l \left(T_s \right) &= \left(39.078 T_s - 1.105 \cdot 10^4 \right)^{-1} \\
\Delta H_{ev} \left(T_s \right) &= \left(2.412 + 1.72 \cdot 10^{-3} T_s - 5.74 \cdot 10^{-6} T_s^2 \right) \cdot 10^6 \\
\sigma \left(T_s \right) &= 0.1051 - 5.36 \cdot 10^{-5} T_s - 1.88 \cdot 10^{-7} T_s^2
\end{aligned}
\tag{48}
$$

Note finally that the coefficients of approximating formulas presented in Table 2 were obtained for water as a liquid coolant. The procedure for derivation of the surrogate model can be repeated for other coolants, if necessary.

5. MULTIDIMENSIONAL POROUS BED

A surrogate model for dryout condition in multidimensional (2D axisymmetric or truly 3D) porous beds can be derived following the procedure presented in Section 3 and demonstrated for a simpler case of 1D porous bed in Section 4. For multidimensional configuration, obtaining each solution point in the parameter space (i.e., determining the dryout heat power or corresponding dryout heat flux at the top of the porous bed) requires numerical solution of governing equations performed repeatedly for various values of the volumetric heating power Q (either gradually increasing it, or applying some search algorithm) to find the value at which dryout occurs. In the non-dimensional form, the dryout condition can be presented as

$$
q_{\mathrm{DHF}} = \Phi \left(\chi, P_{sys}, \Pi_M, \Pi_G \right) \tag{49}
$$

where Π_M denotes model-specific parameters (cf. Eqs. (13), (21), (34)), whereas Π_G denotes a set of geometry parameters describing the porous bed shape.

By following the proposed approach directly, one can determine the asymptotic functions $\Phi_0 \left(\chi, \Pi_M, \Pi_G \right)$ and $\Phi_\infty \left(\chi, \Pi_M, \Pi_G \right)$ describing behavior of (49) at small and large χ, and then determine the interpolant $\hat{\Phi} \left(\hat{\chi}, \Pi_G \right)$. These functions, however, would be geometry-specific, and a new set of functions must be generated for a particular porous bed shape.

A preferable approach is based on the approximate factorization of (49):

$$
\Phi \left(\chi, P_{sys}, \Pi_M, \Pi_G \right) \approx \Phi^0 \left(\chi, P_{sys}, \Pi_M \right) \cdot \Psi \left(\Pi_G \right) \tag{50}
$$

where Φ^0 corresponds to the approximation obtained in Section 4 for 1D porous bed, while $\Psi \left(\Pi_G \right)$ is a shape-specific factor describing the effects of geometry. In this way, the asymptotic formulas and interpolating functions derived for one-dimensional bed are used in the surrogate model for multidimensional bed coolability, reducing significantly the computational expenses required for the derivation of approximating formulas.

Factorization (50) was successfully applied to axisymmetric heat-releasing porous beds (conical, cylindrical, mound-shaped) in [13, 14, 15, 16] with simulations performed on the basis of Reed's drag model. It was shown that, with properly defined shape functions Ψ (depending, for example, on the slope angle of bed surface), non-dimensional dryout heat fluxes Φ^0 obtained

for different particle diameters, porosity, and system pressure, collapse to the same curve as in 1D case. Generalization of this approach to other drag models, and finding representations for the shape functions will be carried out in our future work.

6. CONCLUSIONS

The analysis of dryout conditions performed in this paper enabled us to obtain the general functional form of the dryout heat flux, applicable to internally heated porous beds of various shapes. We considered three drag models available in the literature, validated and widely applied to coolability studies. The main focus of the current paper was to find an efficient way of dryout heat flux calculation. For the well-known problem of dryout heat flux for a one-dimensional top-flooded porous bed, a set of analytical approximating formulas was obtained offering a computationally efficient model.

The real advantages of the proposed approach are connected with development of surrogate models for coolability of multidimensional porous beds. This enables Monte Carlo simulations for quantification of uncertainty in application to assessment of severe accident risk, substituting computationally expensive numerical models with fast surrogate models. Previous experience gained with numerical results obtained for Reed's drag model indicates that the approximating functions obtained for 1D problem can be re-used as a part of such surrogate model for multidimensional beds. Applicability of this approach to other drag models has yet to be studied, and relevant shape factor functions have yet to be derived in a form allowing their application for safety analysis and other engineering purposes.

7. ACKNOWLEDGMENTS

The work is supported by the Swedish Radiation Safety Authority (SSM), Swedish Power Companies, Nordic Nuclear Safety Research (NKS), Swiss Federal Nuclear Safety Inspectorate (ENSI) under the APRI-MSWI program at the Royal Institute of Technology (KTH), Stockholm, Sweden. Support by Russian Ministry of Science and High Education (Project Reg. No. AAAA-A17-117021310385-6) is also acknowledged.

NOMENCLATURE

a_0, b_0, c_0, d_0	coefficients in best-fit approximation (47) for Φ_0 (–)
a_∞, b_∞, c_∞, d_∞	coefficients in best-fit approximation (47) for Φ_∞ (–)
c_χ	exponent in variable transformation (45) (–)
C_1, C_2	constants in the interfacial drag model [7, 8] (–)
Ca	capillary number (–)
DHF	dryout heat flux (W/m^2)
D_b	bubble diameter (m)
d	particle diameter (m)
d_ε	characteristic pore size (m)

$\mathbf{F}$	drag force per unit volume (N/m^3)
Fr	Froude number
$\mathbf{g}$, $g = \lvert\mathbf{g}\rvert$	gravity acceleration vector and absolute value (m/s^2)
H	porous bed height (m)
ΔH_{ev}	latent heat of evaporation (J/kg)
J_1, J_2, J_Γ	characteristic superficial velocities (m/s)
$\mathbf{j}_i$	superficial velocity of *i*-th phase (m/s)
K	permeability (m^2)
K_{ri}	relative permeability of *i*-th phase (–)
L	length (m)
n	exponent in relative permeability
m	exponent in relative passability
P	pressure (Pa)
P_{sys}	prevailing system pressure (bar)
Q	volumetric heat release rate (W/m^3)
q	non-dimensional heat flux (–)
q_{DHF}	non-dimensional dryout heat flux (–)
T_s	saturation temperature (K)
$\mathbf{V}_r$	relative phase velocity (m/s)
W	specific heating power (W/kg)

Greek

α	void fraction, $\alpha = \alpha_v$ (–)
α_i	volume fraction of *i*-th phase (–)
α_*, $\alpha_1 - \alpha_4$	boundaries between flow regimes in models [6–8] (–)
Γ	evaporation rate (kg/m^3·s)
γ	ratio of bubble and particle diameters (–)
ε	porosity (–)
η	passability (m)
η_{ri}	relative passability of *i*-th phase (–)
μ_i	dynamic viscosity of *i*-th phase (Pa·s)
Π_G	set of geometry-specific parameters
Π_M	set of model-specific parameters
ρ_i	density of *i*-th phase (kg/m^3)
ρ_s	solid material density (kg/m^3)
σ	surface tension (N/m)
Φ	functional form of q_{DHF} (–)
Φ_0, Φ_∞	asymptotic form of Φ at small and large χ

χ	non-dimensional porous medium drag parameter (–)
χ_0	coefficient in variable transformation (45) (–)
Ψ	shape-specific function for multidimensional porous bed

Subscripts

i , j	phase (either *l* or *v*)
l	liquid
v	gas phase (vapor)

Superscripts

*	scale
m	modified value in drag model [8]
max	maximum value
top	top horizontal cross-section of porous bed

Accents

~	non-dimensional quantity
^	rescaled non-dimensional quantities
–	transformed variable in fitting formula

8. REFERENCES

1. J.E. Yang, Fukushima Dai-Ichi accident: Lessons learned and future actions from the risk perspectives, Nucl. Eng. Technol. 46 (2014) 27–38. doi:10.5516/NET.03.2014.702.
2. P.Kudinov, S.Galushin, S.Yakush, W.Villanueva, V.-A.Phung, D.Grishchenko, N.Dinh, 2014, "A Framework for Assessment of Severe Accident Management Effectiveness in Nordic BWR Plants," Probabilistic Safety Assessment and Management PSAM 12, June 22-27, 2014, Honolulu, Hawaii, Paper 154.
3. R. Lipinski, A one dimensional particle bed dryout model, ANS Trans., 38 (1981) 386–387.
4. A.Reed, The Effect Of Channeling on the Dryout of Heated Particulate Beds Immersed in a Liquid Pool, *PhD Thesis*, MIT, Cambridge, 1982 .
5. K. Hu, T.G. Theofanous, On the measurement and mechanism of dryout in volumetrically heated coarse particle beds, Int. J. Multiph. Flow. 17 (1991) 519–532. doi:10.1016/0301-9322(91)90047-7.
6. T. Schulenberg, U. Müller, An improved model for two-phase flow through beds of coarse particles, Int. J. Multiph. Flow. 13 (1987) 87–97. doi:10.1016/0301-9322(87)90009-7.
7. V.X. Tung, V.K. Dhir, A hydrodynamic model for two-phase flow through porous media, Int. J. Multiph. Flow. 14 (1988) 47–65. doi:10.1016/0301-9322(88)90033-X.
8. W. Schmidt, Interfacial drag of two-phase flow in porous media, Int. J. Multiph. Flow. 33 (2007) 638–657. doi:10.1016/j.ijmultiphaseflow.2006.09.006.
9. P. Schäfer, M. Groll, R. Kulenovic, Basic investigations on debris cooling, Nucl. Eng. Des. 236 (2006) 2104–2116. doi:10.1016/j.nucengdes.2006.03.033.

10. I. Lindholm, S. Holmström, J. Miettinen, V. Lestinen, J. Hyvärinen, P. Pankakoski, H. Sjövall, Dryout heat flux experiments with deep heterogeneous particle bed, Nucl. Eng. Des. 236 (2006) 2060–2074. doi:10.1016/j.nucengdes.2006.03.036.
11. E. Takasuo, S. Holmström, T. Kinnunen, P.H. Pankakoski, The COOLOCE experiments investigating the dryout power in debris beds of heap-like and cylindrical geometries, Nucl. Eng. Des. 250 (2012) 687–700. doi:10.1016/j.nucengdes.2012.06.015.
12. M. Bürger, M.Buck, W.Schmidt, W.Widmann, Validation and application of the WABE code: Investigations of constitutive laws and 2D effects on debris coolability, Nucl. Eng. Des. 236 (2006) 2164–2188. doi:10.1016/j.nucengdes.2006.03.058.
13. S.E. Yakush, N.T.Lubchenko, P.Kudinov, Risk-informed approach to debris bed coolability issue, in: Int. Conf. Nucl. Eng. Proceedings, ICONE20, 2012: pp. 531–543. doi:10.1115/ICONE20-POWER2012-55256.
14. S.E.Yakush, N.T.Lubchenko, P.Kudinov, 2013, "Surrogate Models for Debris Bed Dryout," Proc. 15th International Topical Meeting on Nuclear Reactor Thermalhydraulics (NURETH 15), May 12–17, 2013, Pisa, Italy, paper NURETH15-278, 16 pp.
15. S. E.Yakush, P.Kudinov , N.T.Lubchenko, 2013, "Risk and Uncertainty Quantification in Debris Bed Coolability," Proc. 15th International Topical Meeting on Nuclear Reactor Thermalhydraulics (NURETH 15), May 12–17, 2013, Pisa, Italy, paper NURETH15-283, 13 pp.
16. S.E.Yakush, N.T.Lubchenko, P.Kudinov. Development and Application of Surrogate Model for Assessment of Ex-Vessel Debris Bed Dryout Probability. International Congress on Advances in Nuclear Power Plants, Nice, France, May 03-06, 2015, Paper 15157, 9 pp.
17. Kudinov, P., Karbojian, A., Ma, W., and Dinh, T.-N. "The DEFOR-S Experimental Study of Debris Formation with Corium Simulant Materials," Nuclear Technology, 170(1), April 2010, pp. 219-230, 2010. https://doi.org/10.13182/NT10-A9460
18. M. Bürger, M. Buck, G. Pohlner, S. Rahman, R. Kulenovic, F. Fichot, W.M. Ma, J. Miettinen, I. Lindholm, K. Atkhen, Coolability of particulate beds in severe accidents: Status and remaining uncertainties, Prog. Nucl. Energy. 52 (2010) 61–75. doi:10.1016/j.pnucene.2009.09.015.
19. G. Pohlner, M. Buck, R. Meignen, P. Kudinov, W. Ma, F. Polidoro, E. Takasuo, Analyses on ex-vessel debris formation and coolability in SARNET frame, Ann. Nucl. Energy. 74 (2014) 50–57. doi:10.1016/j.anucene.2014.07.013.
20. A. I. J. Forrester, A. Sobester, A. J. Keane, Engineering Design via Surrogate Modelling. A Practical Guide. J Wiley & Sons, Chichester, UK (2008).
21. S. Ergun, Fluid flow through packed columns, Chem. Eng. Prog. 48 (1952) 89–94. doi:10.1029/JB088iS01p0B353.
22. E. Loth, T. O'Brien, M. Syamlal, M. Cantero, Effective diameter for group motion of polydisperse particle mixtures, Powder Technol. 142 (2004) 209–218. doi:10.1016/j.powtec.2004.04.033.
23. S. E. Yakush, P. Kudinov, "A Model for Prediction of Maximum Post-Dryout Temperature in Decay-Heated Debris Bed," Proc. 22th International Conference on Nuclear Engineering (ICONE22), Prague, Czech Republic, July 7-11, 2014, paper ICONE22-31214, 11 pp.
24. S. E. Yakush and P. Kudinov, 2017, "Melt Agglomeration Influence on Ex-vessel Debris Bed Coolability," Proc. 17th International Topical Meeting on Nuclear Reactor Thermalhydraulics (NURETH 17), Sept 3–8, 2013, Xi'an, China, paper NURETH17-21455, 14 pp.

25. S. Whitaker, Flow in porous media II: The governing equations for immiscible, two-phase flow, Transp. Porous Media. 1 (1986) 105–125. doi:10.1007/BF00714688.
26. F.E. Torres, Closure of the governing equations for immiscible, two-phase flow: A research comment, Transp. Porous Media. 2 (1987) 383–393. doi:10.1007/BF00136443.
27. S. Whitaker, The closure problem for two-phase flow in homogeneous porous media, Chem. Eng. Sci. 49 (1994) 765–780.
28. D. Lasseux, M. Quintard, S. Whitaker, Determination of permeability tensors for two-phase flow in homogeneous porous media: Theory, Transp. Porous Media. 24 (1996) 107–137. doi:10.1007/BF00139841.
29. D. Lasseux, A. Ahmadi, A.A.A. Arani, Two-Phase inertial flow in homogeneous porous media: A theoretical derivation of a macroscopic model, Transp. Porous Media. 75 (2008) 371–400. doi:10.1007/s11242-008-9231-y.
30. R. Clavier, N. Chikhi, F. Fichot, M. Quintard, Modeling of inertial multi-phase flows through high permeability porous media: Friction closure laws, Int. J. Multiph. Flow. 91 (2017) 243–261. doi:10.1016/j.ijmultiphaseflow.2017.02.003.
31. D. Magallon, I. Huhtiniemi, Corium melt quenching tests at low pressure and subcooled water in FARO, Nucl. Eng. Des. 204 (2001) 369–376. doi:10.1016/S0029-5493(00)00318-6.
32. P. Kudinov, A. Karbojian, C.T. Tran, W. Villanueva, Agglomeration and size distribution of debris in DEFOR-A experiments with Bi2O3-WO3 corium simulant melt, Nucl. Eng. Des. 263 (2013) 284–295. doi:10.1016/j.nucengdes.2013.06.011.
33. A. D. Polyanin, V. V. Dilman, Methods of Modeling Equations and Analogies in Chemical Engineering, CRC Press/Begell House, Boca Raton–Ann Arbor, 1994.
34. IAPWS, The International Association for the Properties of Water and Steam, http://www.iapws.org.